Theoretical Chemistry Accounts (2018) 137:33
https://doi.org/10.1007/s00214-018-2221-4

REGULAR ARTICLE

The isotope effect on charge transport for bithiophene and di(*n*-hexyl)-bithiophene: impacts of deuteration position, deuteration number and side chain substitution position

Yuqian Jiang[1,2] · **Zhigang Shuai**[2] · **Minghua Liu**[1]

Received: 25 August 2017 / Accepted: 12 February 2018 / Published online: 21 February 2018

Abstract
The isotope effect on charge transport had been proposed to judge the transport mechanism in organic semiconductors. By using quantum nuclear tunneling model, we found that isotopic substitution could reduce mobility. For deeply understanding the impacts of the isotopic substitution position, substitution number and even molecular structure on the isotope effect, we take 2,2′-bithiophene and its dihexyl substitutions as examples to study the deuteration effect on hole transport. For deuterated–bithiophene, the isotope effect is linearly increasing with deuteration number. However, when the number is identical, deuteration on 5(5′)-position of thiophene will lead to stronger isotope effect than 3(3′)- or 4(4′)-position, since the reorganization energy contributed by 5-position hydrogen atoms is larger. For di(*n*-hexyl)-bithiophene isomers, 5,5′-dihexyl substitution also exhibits the strongest isotope effect after hexyl-deuteration or all-deuteration, due to the larger reorganization energy contributed by hexyl group in 5(5′)-position rather than 3(3′)- and 4(4′)-positions. Our calculation indicates that for identical system, the isotope effect is closely related to the number and position of isotopic atoms, while for isomers, the isotope effect is also related to the molecular configuration, such as the position of side chain substitution.

Keywords Charge transport · Nuclear tunneling · Isotope effect · Deuteration · Bithiophene

1 Introduction

Organic semiconductors have long been used to fabricate molecular electronics and photonics, such as organic field-effect transistors (OFET), organic light-emitting diodes (OLED) and organic solar cells (OSC) [1–4], due to their unique optoelectronic properties [5–7]. Charge carrier mobility, as such a crucial factor on the performance of electronic devices, has attracted great attention to experimentalists and theorists. Tremendous progresses on materials design and device fabrication have been achieved for improving carrier mobility. Even so, the charge transport mechanism in organic semiconductors is still in controversy up to now.

To describe the transport mechanism, numerous theories have been proposed such as semiclassical Marcus theory [8–11], Boltzmann band-like transport theory [10, 12, 13] and polaron models [14–19]. However, some exotic experimental phenomena still could not be understood. For example, one recent experiment indicates that the transport in tetracene is governed by the hopping mechanism rather than band model which people normally considered [20]. Moreover, in situ charge modulation spectroscopy on OFET with TIPS-pentacene as the active layer also indicates that the transporting carriers come from localized charges, even at very low temperature, while the mobility decreases with temperature [21]. For understanding such exotic transport behavior, quantum nuclear tunneling of localized charge hopping [22, 23] was proposed to account for such paradoxical phenomena for TIPS-pentacene [24]. Such nuclear tunneling effect has been adopted in several charge transport

✉ Yuqian Jiang
jiangyq@nanoctr.cn

✉ Zhigang Shuai
zgshuai@tsinghua.edu.cn

[1] Laboratory for Nanosystem and Hierarchy Fabrication, CAS Center for Excellence in Nanoscience, National Center for Nanoscience and Technology, Beijing 100084, People's Republic of China

[2] MOE Key Laboratory of Organic OptoElectronics and Molecular Engineering, Department of Chemistry, Tsinghua University, Beijing 100084, People's Republic of China

models [25–30] to well elucidate the transport mechanism in organic semiconductors and polymers.

To illustrate the role of nuclear tunneling on charge transport, we suggested using isotope effect (IE) on charge mobility [31, 32]. Our previous calculation results indicate that negative IE will exist if nuclear-tunneling-assisted hopping is the mechanism, since heavier atoms can weaken the quantum nuclear tunneling effect, approaching the semiclassical end where there is no IE. Conversely, it is absent in semiclassical Marcus hopping process or in band-like transport process when acoustic phonon scattering dominates. Our theoretical results also show coincidence with earlier experimental observations [33], where Morel and Hermann observed 10% negative IE in the c' direction and zero effect in a and b directions for electron mobility in all-deuterated anthracene in 1973. There were also some other theories and experiments proposed for IE on charge transport [34–37], and even positive IE on mobility was found experimentally and theoretically [34, 35]. However, the quantum nuclear tunneling model with considering all normal modes bath that we used can fully describe optical phonon scattering and result in exact IE on charge transport. Therefore, we believe that isotopic substitution will decrease carrier mobility when optical phonon scattering is not ignorable.

In this work, we intend to further study the relationship between IE on charge transport and molecular structures fundamentally. Oligothiophenes as typical p type organic materials have been widely applied in fabricating OFET [38–42]. Though the hole mobility of oligothiophenes is no larger than 1 $cm^2\ V^{-1}\ s^{-1}$, the specific characteristics of weak hydrogen bondings, π–π stacking and sulfur–sulfur interactions originating from the high polarizability of sulfur electrons in the thiophene rings still attract numerous investigations for oligothiophenes and their derivatives. The rotation of carbon–carbon single bond connecting two neighboring thiophene rings makes oligothiophenes possess relatively large charge reorganization energy, which are much larger than intermolecular transfer integrals, so that the charge transport in oligothiophene was generally dealt with hopping model [43–45]. Here, we employ the quantum hopping model with nuclear tunneling effect and take 2,2′-bithiophene (2T) and di(n-hexyl)-bithiophene (2HT) isomers (Scheme 1) as example, to thoroughly study the internal relation between deuterium effect and molecular structures. We calculate IE on hole transport for all kinds of deuterated-2Ts and find that IE is linearly increasing with deuteration number. All-deuteration can reduce charge transfer (CT) rate by 7%. However, when deuteration numbers are identical, 2T with 5-position or/and 5′-position deuterated possesses the strongest IE. We then compute hexyl-deuteration and all-deuteration effects for four different 2HT isomers, most of which are stronger than 10%. Wherein it is hexyl substitution on 5,5′-positions of which deuteration can cause the most

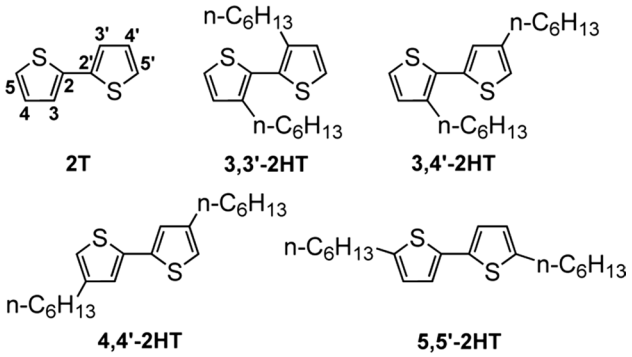

Scheme 1 Molecular structures of 2,2′-bithiophene (2T) and four di(n-hexyl)-bithiophenes (2HTs)

decrease on the CT rate, which are 23 and 25%, respectively, for hexyl-deuteration and all-deuteration. With decomposing reorganization energy into normal modes and internal coordinates, it is found that the larger reorganization energy contributed by isotopic atoms leads to the stronger IE, which agrees well with our previous study [31]. Our calculations further indicate that for identical system IE is closely related to the number and position of isotopic atoms, while for different isomers it is also related to molecular structures.

2 Theoretical methodology

The quantum CT rate from one molecule to another can be derived from Fermi's golden rule which can be expressed as

$$W_{i\to f} = \frac{2\pi}{\hbar^2}\left|\left\langle \Phi_f\middle|H'\middle|\Phi_i\right\rangle\right|^2 \sum_{\upsilon}\sum_{\upsilon'} P_{i\upsilon}\left|\left\langle \Theta_{f\upsilon'}\middle|\Theta_{i\upsilon}\right\rangle\right|^2 \delta\left(\omega_{f\upsilon',i\upsilon}\right), \tag{1}$$

where $\Phi_{i(f)}$ and $\Theta_{i(f)}$ represent the electronic and vibrational wave functions separately, and $P_{i\upsilon}$ donates the Boltzmann distribution function

$$P_{i\upsilon} = \left[\sum_{\upsilon}\exp\left(\frac{-E_{i\upsilon}}{kT}\right)\right]^{-1}\exp\left(\frac{-E_{i\upsilon}}{kT}\right). \tag{2}$$

Under the displaced harmonic oscillator approximation [22, 46], Eq. (1) can be translated into

$$k^{QM} = \frac{|V|^2}{\hbar^2}\int_{-\infty}^{\infty} \mathrm{d}t \exp\left\{-\sum_j S_j\left[\left(2\bar{n}_j+1\right) - \bar{n}_j e^{-i\omega_j t} - \left(\bar{n}_j+1\right)e^{i\omega_j t}\right]\right\}. \tag{3}$$

Here, $V = \left|\left\langle \Phi_f\middle|H'\middle|\Phi_i\right\rangle\right|$ is the intermolecular transfer integral, $\bar{n}_j = 1/[\exp(\hbar\omega_j/k_BT) - 1]$ is the occupation number for the jth vibrational mode with frequency ω_j, and S_j is the Huang–Rhys factor relating of the jth mode:

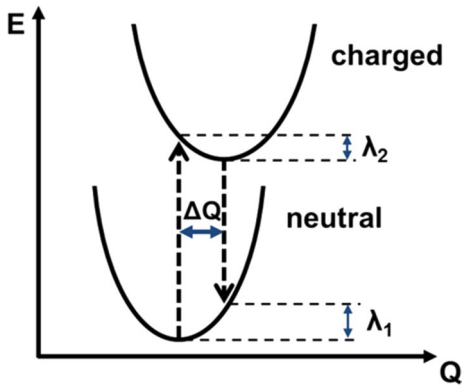

Fig. 1 Schematic representation of the potential energy surface of the neutral and charged molecules. ΔQ is the normal mode displacement. λ_1 and λ_2 are reorganization energies for neutral and charged molecules, respectively

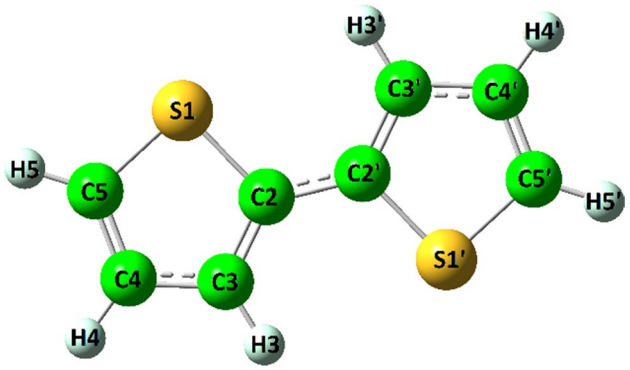

Fig. 2 Molecule structure of 2T

$$S_i = \frac{\omega_i}{2\hbar}\left(\Delta Q_i\right)^2, \tag{4}$$

where ΔQ_i represents the displacement along the ith normal mode coordinate between the equilibrium positions of charged state and neutral state (Fig. 1). The reorganization energy in geometry between the neutral and charged states through the kth intramolecular vibrational mode is determined by

$$\lambda_k = S_k \hbar \omega_k, \tag{5}$$

and the total reorganization energy for neutral (λ_1) or charged molecule (λ_2) is the sum over all modes at each state as

$$\lambda_{1(2)} = \sum\nolimits_j \lambda_j^{1(2)} = \sum\nolimits_j S_j^{1(2)} \hbar \omega_j^{1(2)}. \tag{6}$$

In general, the potential energy surface can be expanded with internal coordinates around the equilibrium geometry as

$$V = V_0 + \frac{1}{2}\mathbf{S}^{\mathrm{T}}\mathbf{F}_{\mathrm{int}}\mathbf{S}. \tag{7}$$

Here, V_0 is the potential energy at the equilibrium geometry and normally set as $V_0 = 0$. $\mathbf{S}$ represents the molecular vibrations via rectilinear internal coordinates $\mathbf{R}$

$$\mathbf{S} = \mathbf{B}(\mathbf{R} - \mathbf{R}_0), \tag{8}$$

where $\mathbf{B}$ is $n_r \times 3N_{\mathrm{nuc}}$ Wilson $\mathbf{B}$ matrix, n_r and N_{nuc} are the number of curvilinear internal coordinates and nuclei separately. $\mathbf{S}$ is approximately equal to the change of curvilinear internal coordinates $\mathbf{z}$:

$$\mathbf{S} \approx \mathbf{z} - \mathbf{z}_0 = \Delta\mathbf{z}. \tag{9}$$

Since the reorganization energy is actually the potential energy difference, the reorganization energy can finally be projected onto curvilinear internal coordinates as

$$\lambda = \frac{1}{2}\Delta\mathbf{z}^{\mathrm{T}}\mathbf{F}_{\mathrm{int}}\Delta\mathbf{z} = \sum_{i=1}^{n_r}\left(\frac{1}{2}f_{\mathrm{int},i,i}\left(\Delta z_i\right)^2 + \frac{1}{2}\sum_{j(\neq 1)}^{n_r} f_{\mathrm{int},i,i}\Delta z_i \Delta z_j\right) = \sum_{i=1}^{n_r}\lambda_i. \tag{10}$$

λ_i can be regarded as the reorganization energy contributed by the ith internal coordinate.

We assume the same crystal structures for different isotope substitutions since they have the same equilibrium geometries, and isotope substitution does not modify the intermolecular integral V. Here, the IE on CT rate is studied instead of the IE on mobility, and the IE between two molecules can be expressed as

$$\frac{k_H - k_L}{k_L} = \frac{\int_{-\infty}^{\infty} \mathrm{d}t \exp\left\{-\sum_j S_j^H\left[\left(2\bar{n}_j^H + 1\right) - \bar{n}_j^H e^{-i\omega_j^H t} - \left(\bar{n}_j^H + 1\right)e^{i\omega_j^H t}\right]\right\}}{\int_{-\infty}^{\infty} \mathrm{d}t \exp\left\{-\sum_j S_j^L\left[\left(2\bar{n}_j^L + 1\right) - \bar{n}_j^L e^{-i\omega_j^L t} - \left(\bar{n}_j^L + 1\right)e^{i\omega_j^L t}\right]\right\}} - 1, \tag{11}$$

where k_L and k_H are the CT rates for the light and heavy isotopically substituted systems separately. According to Eq. (11), all CT rates between dimers in crystal have the same IE value, so that the IE on mobility is proportional to the IE on CT rate due to the Einstein formula $\mu = eD/k_{\mathrm{B}}T$. Moreover, referring to our previous work [31], the IE on mobility is nearly equal to the IE on CT rate. Thus, the study of IE on CT rate can interpret the isotope effect on charge transport in organic semiconductors.

Density functional theory (DFT) is applied to calculate molecular parameters appeared in Eq. (3) with Gaussian 09 package [47]. The neutral and cation geometries of 2T and 2HTs are optimized with B3LYP functional [48, 49] and 6-31G(d) basis set in C_s symmetry to keep planar as the same in crystal [50, 51], for studying their intrinsic charge transport properties. With the help of DUSHIN program [52], the corresponding Huang–Rhys factors and the reorganization energies are obtained for every normal modes under the displaced harmonic oscillator approximation, and the reorganization energies of all internal coordinates are

also achieved. Our calculations show that the total reorganization energies are invariable after isotope substituting for the case of identical electronic structures of isotopic substitutions. For the rigid systems, the integral part in Eq. (3) or (11) is hard to converge without a decay factor. Thus, we add a Lorentzian $e^{-\Gamma|t|}$ factor with a very small broadening $\Gamma = 2\ \mathrm{cm}^{-1}$ for all systems to guarantee the convergence, which can be regarded as dissipation broadening from the environments.

3 Results and discussion

3.1 Deuteration effect on 2T

We first investigate how the number and position of deuteration influence hole transport for 2T. Considering the C_s symmetry of 2T molecule, there are totally 35 different deuterated-2Ts (2T-d_n), from one-deuterated to completely deuterated, as listed in Table 1.

By employing Eq. (11) with considering all intramolecular electron–phonon coupling, the isotope effects on hole transport for all 2T-d_n are calculated and presented in Fig. 3. It is easy to find that all kinds of deuterations make CT rate and mobility decrease, and all-deuterated 2T (2T-d_6) (**1**) exhibits the strongest IE which reduces the CT rate by 7%. Besides, the IE is overall linearly strengthened with the increasing number of hydrogen deuterated, of which the similar effect has been found in the triplet-state decay process of naphthalene by Lin et al. [53]. This phenomenon can be easily understood by normal mode analysis. By projecting reorganization energy onto normal modes, we find that hydrogen atoms mainly participate in carbon–hydrogen

Table 1 Index and deuteration position for all deuterated-2Ts. The labels are shown in Fig. 2

Index	Deuteration positions	Index	Deuteration positions	Index	Deuteration positions
1	3–5, 3′–5′	**14**	3–5	**24**	3, 4
2	3–5, 3′, 4′	**15**	3, 4, 3′	**25**	3, 5
3	3–5, 3′, 5′	**16**	3, 4, 4′	**26**	4, 5
4	3–5, 4′, 5′	**17**	3, 4, 5′	**27**	3, 3′
5	3–5, 3′	**18**	3, 5, 3′	**28**	3, 4′
6	3–5, 4′	**19**	3, 5, 4′	**29**	3, 5′
7	3–5, 5′	**20**	3, 5, 5′	**30**	4, 4′
8	3, 4, 3′, 4′	**21**	4, 5, 3′	**31**	4, 5′
9	3, 4, 3′, 5′	**22**	4, 5, 4′	**32**	5, 5′
10	3, 4, 4′, 5′	**23**	4, 5, 5′	**33**	3
11	3, 5, 3′, 5′			**34**	4
12	3, 5, 4′, 5′			**35**	5
13	4, 5, 4′, 5′				

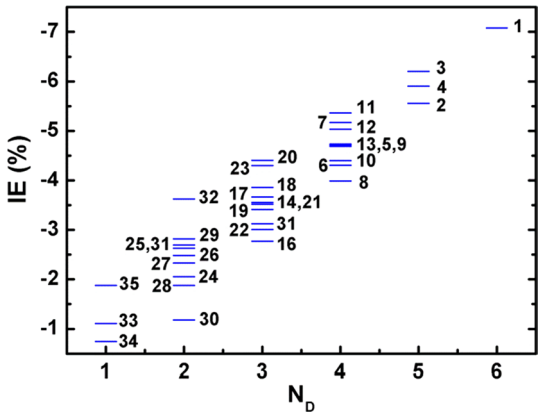

Fig. 3 Isotopic effect (IE) for all 2T-d_n with different number of H atoms deuterated (N_D). The index of each deuterated-2T is labeled

(C–H) bending vibrations (Table 2). The vibrational modes with the most significant contribution to the reorganization energy as shown in Fig. 4 also indicate that all six H atoms take part in the vibrations. Therefore, with deuterium atoms number increasing, heavier nuclei lead to lower frequencies of normal modes. Since the reorganization energy is independent on isotopic substitution, lower frequencies make electron–phonon coupling stronger, but nuclear tunneling effect weaker, then resulting to decreased CT rate.

However, when the numbers of deuterated atoms are identical, IEs of different deuterated-2T are somehow different from each other. For three one-deuterated 2T (2T-d_1) (**33**, **34** and **35**), the order of IE is: 2T-d_1(5) (**35**) > 2T-d_1(3) (**33**) > 2T-d_1(4) (**34**), meaning that deuteration on 5-position leads to the largest CT rate decrease, while deuteration on 4-position leads to the smallest. For other 2T-d_n systems with the same deuteration number, their IEs also rely on such position effect. For example, deuteration on 5 and 5′ positions, namely 2T-d_2(5,5′) (**32**) results to the largest reduction on CT rate among all 2T-d_2 systems, while 2T-d_2(4,4′) (**30**) possesses the weakest IE. For three hydrogens deuterated substitutions, 2T-d_3(3,5,5′) (**20**) exhibits the strongest IE, while 2T-d_3(3,4,4′) (**16**) shows the weakest effect. For understanding such position effect, we decompose the reorganization energy into internal coordinates for 2T according to Eq. (10), as listed in Table 3.

The reorganization energy of each internal coordinate listed in Table 3 illustrates that C and S nuclei contribute appreciably to the reorganization energy, while no H nuclei shows important contribution to charge reorganization except H5 and H5′ which contribute to a certain degree by participating in the C–C–H bending vibration. Thus, deuteration on H5 or H5′ can cause the largest increase on Huang–Rhys factor and lead to the strongest IE. This phenomenon agrees with our previous study [31] that the noticeable IE on charge transport only happens when the isotopic

Table 2 Frequencies (ω), Huang–Rhys factors (S), reorganization energies (λ) and vibration types of all vibrational modes with $\lambda > 1$ meV for neutral and cation 2T

Neutral				Cation			
ω (cm^{-1})	S	λ (meV)	Vib. types[a]	ω (cm^{-1})	S	λ (meV)	Vib. types[a]
291.68	0.1831	6.62	iii	294.14	0.1743	6.36	iii
381.36	0.3535	16.72	iii	382.97	0.3567	16.94	iii
681.36	0.1470	12.42	iii	681.66	0.2339	19.76	iii
741.93	0.0823	7.57	iii, iv	710.64	0.0367	3.23	iii, iv
862.88	0.1255	13.43	iii, iv	875.97	0.1034	11.23	iii, iv
1079.99	0.071	9.50	i, ii	1107.68	0.0077	1.05	i, ii
1114.61	0.0251	3.47	i, ii	1117.55	0.0545	7.55	i, ii
1243.60	0.0642	9.90	i, ii, iv	1233.06	0.1156	17.68	i, ii, iv
1414.90	0.0078	1.36	i, ii	1317.88	0.0664	10.85	i, ii
1503.90	0.4548	84.79	i, ii	1439.99	0.1126	20.11	i, ii
1609.94	0.0848	16.92	i, ii	1484.82	0.0543	10.00	i, ii
				1558.61	0.2846	55.00	i, ii

[a]Vibration types: (i) C–C stretching vibration; (ii) C–H in-plane bending vibration; (iii) thiophene ring in-plane bending vibration; (iv) C–S stretching vibration. The major contributed vibration types of each mode are underlined

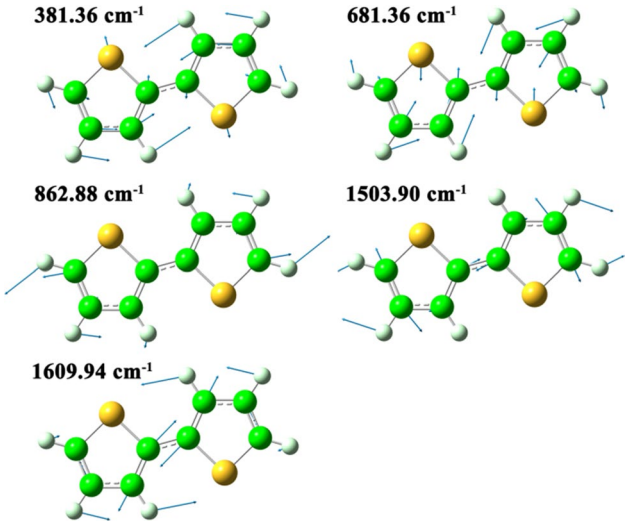

Fig. 4 Five vibrational modes of neutral 2T with the most significant contribution to the reorganization energy

substitution positions are involved actively in the vibration with appreciable contribution to the charge reorganization energy. Therefore, the theoretical calculations on the series of deuterated-2Ts demonstrate that IE on charge transport is closely related to the number as well as the position of deuteration.

3.2 Deuteration effect on 2HT

We then extend our calculation on 2HT isomer systems. Four kinds of 2HTs have been considered here as presented in Scheme 1. The deuteration effects for hexyl-deuteration and all-deuteration of each 2HT have been calculated. The theoretical results shown in Fig. 5 illustrate that all the 2HTs exhibit considerable negative IEs after hexyl-deuteration or all-deuteration, most of which are larger than 10%. Wherein the IEs of 5,5′-2HT are strongest, where hexyl-deuteration and all-deuteration reduce CT rate by 23 and 25% separately. This phenomenon shows coincidence with 2T-d_2 systems

Table 3 Decomposed reorganization energy (λ) of all internal coordinates with $\lambda > 1$ meV for neutral 2T

Internal coordinates	λ (meV)		
	Neutral	Cation	Total
B (C2–C2′)	30.09	36.26	66.35
B (C2–C3)	25.60	21.22	46.82
B (C2′–C3′)	25.32	21.04	46.36
B (C3–C4)	17.57	19.69	37.26
B (C3′–C4′)	17.44	19.56	37.01
B (C4–C5)	18.86	16.53	35.38
B (C4′–C5′)	18.63	16.35	34.97
A (S1–C5–C4)	4.90	4.44	9.34
A (S1′–C5′–C4′)	4.67	4.23	8.90
B (S1–C5)	2.16	2.92	5.09
B (S1′–C5′)	1.95	2.64	4.96
A (C2–S1–C5)	2.21	2.75	4.93
A (C2′–S1′–C5′)	2.20	2.73	4.58
A (C4–C5–H5′)	**2.16**	**1.98**	**4.13**
A (C4′–C5′–H5′)	**1.99**	**1.82**	**3.82**
B (S1′–C2′)	1.75	1.13	2.88
B(S1–C2)	1.72	1.09	2.80
A (C3–C2–C2′)	1.02	1.12	2.14
A (C2–C2′–C3′)	1.00	1.10	2.10

The internal coordinates with H participating are in bold

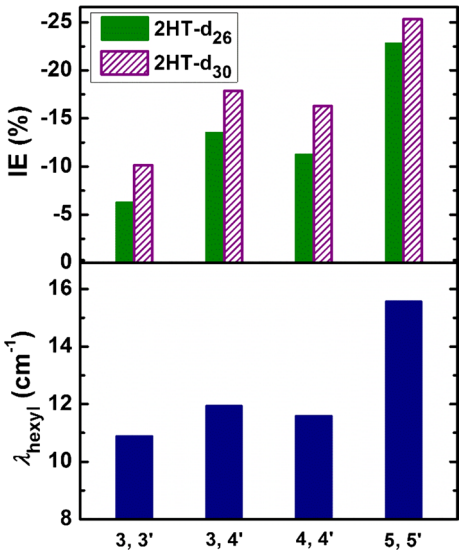

Fig. 5 Isotope effects (IE) of hexyl-deuterated 2HTs (2HT-d_{26}) and all-deuterated 2HTs (2HT-d_{30}), as well as the reorganization energy contributed by hexyl side chains (λ_{hexyl}) for four 2HTs

that deuteration on H5 and H5′ results to the strongest IE. Considering the close relation between IE and reorganization energy contributed by isotopically substituted nuclei, the reorganization energy of each 2HT has also been projected onto internal coordinates and the total contribution made by hexyl side chains has been presented in Fig. 5. It shows that the reorganization energy contributed by hexyl side chains (λ_{hexyl}) is distinctly different in four 2HTs and the IE is positively correlated with λ_{hexyl} for different systems. The cause that 5,5′-2HT possesses biggest λ_{hexyl} should be attributed to the largest contribution of H5(H5′) to charge reorganization in 2T system. Considering that the nuclei mass increases are the same after hexyl-deuteration or all-deuteration for different 2HTs, the vibrational frequency reductions should be similar. Thus, larger λ_{hexyl} can lead to more Huang–Rhys factor increase, then resulting to stronger IE. Therefore, for different 2HTs, hexyl-deuteration or all-deuteration effect is related to the hexyl-substituted positions.

4 Conclusion

We investigate the intrinsic deuterium effect on hole transport for 2T and 2HTs by quantum nuclear tunneling quantum model. For 2T, with deuteration number increasing, the IE will increase linearly, since all H atoms belong to aromatic H and participate in C–H bending vibrations. All-deuteration on 2T can reduce CT rate by 7%. According to normal mode analysis, C–H in-plane bending vibrations make significant contribution to charge reorganization. Therefore, larger number of deuteration on 2T can cause greater impact on C–H bending vibrations and lead to stronger IE. When the number of deuterated atoms is the same, 2T with 5- or/and 5′-position deuterated presents the strongest IE, because the reorganization energy contributed from 5(5′)-position H is larger than that from any other H atoms. For four different 2HT systems, deuteration on either hexyl groups or whole molecules can lead to appreciable negative IEs, most of which are stronger than 10%. Wherein deuteration on 5,5′-2HT can cause the most decrease on the CT rate and mobility, which are 23 and 25%, respectively, for hexyl-deuterated and all-deuterated systems. The reorganization energy contributed from hexyl groups for four 2HTs points out that only vibrations involved by isotopic atoms with larger reorganization energy can lead to larger IE. Moreover, our calculations indicate that for one system IE is closely related to the number and position of isotopic atoms, while for isomers IE is also related to the molecular structure, such as side chain substituted position. Furthermore, by studying the IE on mobility for 2T and 2HT, the nuclear tunneling effect in charge transport may be deeply understood.

Acknowledgements This work is supported by National Natural Science Foundation of China (Grant No. 21603043).

References

1. Yuan YB, Giri G, Ayzner AL, Zoombelt AP, Mannsfeld SCB, Chen JH, Nordlund D, Toney MF, Huang JS, Bao ZN (2014) Ultra-high mobility transparent organic thin film transistors grown by an off-centre spin-coating method. Nat commun 5:3005–3013
2. Gélinas S, Rao A, Kumar A, Smith SL, Chin AW, Clark J, van der Poll TS, Bazan GC, Friend RH (2014) Ultrafast long-range charge separation in organic semiconductor photovoltaic diodes. Science 343:512–516
3. Zhang L, Fonari A, Liu Y, Hoyt ALM, Lee H, Granger D, Parkin S, Russell TP, Anthony JE, Bredas JL, Coropceanu V, Briseno AL (2014) Bistetracene: an air-stable, high-mobility organic semiconductor with extended conjugation. J Am Chem Soc 136:9248–9251
4. Zhang Q, Li J, Shizu K, Huang S, Hirata S, Miyazaki H, Adachi C (2012) Design of efficient thermally activated delayed fluorescence materials for pure blue organic light emitting diodes. J Am Chem Soc 134:14706–14709
5. Deng CM, Niu YL, Peng Q, Shuai ZG (2010) Electronic structures and spectroscopic properties of group-14 metalloles MPh6 (M = Si, Ge, Sn). Acta Phys Chim Sin 26:1051–1058
6. Shuai ZG, Xu W, Peng Q, Geng H (2013) From electronic excited state theory to the property predictions of organic optoelectronic materials. Sci China Chem 56:1277–1284
7. Shi QH, Peng Q, Sun SR, Shuai ZG (2013) Vibration correlation function investigation on the phosphorescence quantum efficiency and spectrum for blue phosphorescent Ir(III) complex. Acta Chim Sin 71:884–891
8. Chen HY, Chao I (2006) Toward the rational design of functionalized pentacenes: reduction of the impact of functionalization on the reorganization energy. ChemPhysChem 7:2003–2007
9. Chai S, Wen SH, Huang JD, Han KL (2011) Density functional theory study on electron and hole transport properties of organic

pentacene derivatives with electron-withdrawing substituent. J Comput Chem 32:3218–3225
10. Kobayashi H, Kobayashi N, Hosoi S, Koshitani N, Murakami D, Shirasawa R, Kudo Y, Hobara D, Tokita Y, Itabashi M (2013) Hopping and band mobilities of pentacene, rubrene, and 2,7-dioctyl[1] benzothieno [3,2-b][1] benzothiophene (C8-BTBT) from first principle calculations. J Chem Phys 139:014707–014714
11. Deng WQ, Goddard WA (2004) Predictions of hole mobilities in oligoacene organic semiconductors from quantum mechanical calculations. J Phys Chem B 108:8614–8621
12. Tang L, Long MQ, Wang D, Shuai ZG (2009) The role of acoustic phonon scattering in charge transport in organic semiconductors: a first-principles deformation-potential study. Sci China, Ser B: Chem 52:1646–1652
13. Cheng YC, Silbey RJ, da Silva Filho DA, Calbert JP, Cornil J, Brédas JL (2003) Three-dimensional band structure and bandlike mobility in oligoacene single crystals: a theoretical investigation. J Chem Phys 118:3764–3774
14. Hannewald K, Bobbert P (2005) Ab-initio theory of charge transport in organic crystals. Phys Semi Part B 772:1101–1104
15. Troisi A (2007) Prediction of the absolute charge mobility of molecular semiconductors: the case of rubrene. Adv Mater 19:2000–2004
16. Troisi A, Orlandi G (2006) Charge-transport regime of crystalline organic semiconductors: diffusion limited by thermal off-diagonal electronic disorder. Phys Rev Lett 96:086601–086604
17. Troisi A, Orlandi G (2006) Dynamics of the intermolecular transfer integral in crystalline organic semiconductors. J Phys Chem A 110:4065–4070
18. Wang LJ, Peng Q, Li QK, Shuai ZG (2007) Roles of inter- and intramolecular vibrations and band-hopping crossover in the charge transport in naphthalene crystal. J Chem Phys 127:044506–044514
19. Jiang YQ, Xu H, Zhao N, Peng Q, Shuai ZG (2014) Spectral signature of intrachain and interchain polarons in donor-acceptor copolymers. Acta Chim Sin 72:201–207
20. Lee B, Chen Y, Fu D, Yi H, Czelen K, Najafov H, Podzorov V (2013) Trap healing and ultralow-noise Hall effect at the surface of organic semiconductors. Nat Mater 12:1125–1129
21. Sakanoue T, Sirringhaus H (2010) Band-like temperature dependence of mobility in a solution-processed organic semiconductor. Nat Mater 9:736–740
22. Nan GJ, Yang XD, Wang LJ, Shuai ZG, Zhao Y (2009) Nuclear tunneling effects of charge transport in rubrene, tetracene, and pentacene. Phys Rev B 79:115203–115211
23. Shuai ZG, Geng H, Xu W, Liao Y, Andre JM (2014) From charge transport parameters to charge mobility in organic semiconductors through multiscale simulation. Chem Soc Rev 43:2662–2679
24. Geng H, Peng Q, Wang LJ, Li H, Liao Y, Ma Z, Shuai ZG (2012) Toward quantitative prediction of charge mobility in organic semiconductors: tunneling enabled hopping model. Adv Mater 24:3568–3572
25. Gorham-Bergeron E, Emin D (1977) Phonon-assisted hopping due to interaction with both acoustical and optical phonons. Phys Rev B 15:3667–3680
26. Ulstrup J, Jortner J (1975) The effect of intramolecular quantum modes on free energy relationships for electron transfer reactions. J Chem Phys 63:4358–4368
27. Asadi K, Kronemeijer AJ, Cramer T, Jan Anton Koster L, Blom PWM, de Leeuw DM (2013) Polaron hopping mediated by nuclear tunnelling in semiconducting polymers at high carrier density. Nat commun 4:1710–1717
28. Yuen JD, Menon R, Coates NE, Namdas EB, Cho S, Hannahs ST, Moses D, Heeger AJ (2009) Nonlinear transport in semiconducting polymers at high carrier densities. Nat Mater 8:572–575
29. Kronemeijer AJ, Huisman EH, Katsouras I, van Hal PA, Geuns TCT, Blom PWM, van der Molen SJ, de Leeuw DM (2010) Universal scaling in highly doped conducting polymer films. Phys Rev Lett 105:156604–156607
30. Rodin AS, Fogler MM (2010) Apparent Power-Law Behavior of Conductance in Disordered Quasi-One-Dimensional Systems. Phys Rev Lett 105:106801–106804
31. Jiang YQ, Geng H, Shi W, Peng Q, Zheng XY, Shuai ZG (2014) Theoretical prediction of isotope effects on charge transport in organic semiconductors. J Phys Chem Lett 5:2267–2273
32. Jiang YQ, Peng Q, Geng H, Ma H, Shuai ZG (2015) Negative isotope effect for charge transport in acenes and derivatives: a theoretical conclusion. Phys Chem Chem Phys 17:3273–3280
33. Mey W, Sonnonstine TJ, Morel DL, Hermann AM (1973) Drift mobility of holes and electrons in perdeuterated anthracene single crystals. J Chem Phys 58:2542–2546
34. Munn RW, Nicholson JR, Siebrand W, Williams DF (1970) Evidence for an isotope effect on electron drift mobilities in anthracene crystals. J Chem Phys 52:6442–6443
35. Munn RW, Siebrand W (1970) Theory of charge carrier transport in aromatic hydrocarbon crystals. J Chem Phys 52:6391–6406
36. Schein LB, McGhie AR (1979) Band-hopping mobility transition in naphthalene and deuterated naphthalene. Phys Rev B 20:1631–1639
37. Xie W, McGarry KA, Liu F, Wu Y, Ruden PP, Douglas CJ, Frisbie CD (2013) High-mobility transistors based on single crystals of isotopically substituted rubrene-d28. J Phys Chem C 117:11522–11529
38. Mannebach EM, Spalenka JW, Johnson PS, Cai Z, Himpsel FJ, Evans PG (2013) High hole mobility and thickness-dependent crystal structure in α, ω-dihexylsexithiophene single-monolayer field-effect transistors. Adv Funct Mater 23:554–564
39. Facchetti A, Mushrush M, Yoon M-H, Hutchison GR, Ratner MA, Marks TJ (2004) Building blocks for *n* type molecular and polymeric electronics. Perfluoroalkyl-versus alkyl-functionalized oligothiophenes (nT; $n = 2 - 6$). Systematics of thin film microstructure, semiconductor performance, and modeling of majority charge injection in field-effect transistors. J Am Chem Soc 126:13859–13874
40. Horowitz G, Garnier F, Yassar A, Hajlaoui R, Kouki F (1996) Field-effect transistor made with a sexithiophene single crystal. Adv Mater 8:52–54
41. Dodabalapur A, Torsi L, Katz HE (1995) Organic transistors: two-dimensional transport and improved electrical characteristics. Science 268:270–271
42. Mannsfeld SCB, Locklin J, Reese C, Roberts ME, Lovinger AJ, Bao Z (2007) Probing the Anisotropic field-effect mobility of solution-deposited dicyclohexyl-α-quaterthiophene single crystals. Adv Funct Mater 17:1617–1622
43. Yang X, Wang L, Wang C, Long W, Shuai Z (2008) Influences of crystal structures and molecular sizes on the charge mobility of organic semiconductors: oligothiophenes. Chem Mater 20:3205–3211
44. Navamani K, Saranya G, Kolandaivel P, Senthilkumar K (2013) Effect of structural fluctuations on charge carrier mobility in thiophene, thiazole and thiazolothiazole based oligomers. Phys Chem Chem Phys 15:17947–17961
45. Duan Y-A, Geng Y, Li H-B, Tang X-D, Jin J-L, Su Z-M (2012) Theoretical study on charge transport properties of cyanovinyl-substituted oligothiophenes. Org Electron 13:1213–1222
46. Lin SH, Chang CH, Liang KK, Chang R, Shiu YJ, Zhang JM, Yang TS, Hayashi M, Hsu FC (2002) Ultrafast dynamics and spectroscopy of bacterial photosynthetic reaction centers. Adv Chem Phys 121:1–88

47. Frisch MJ, Trucks GW, Schlegel HB (2004) Gaussian 03. Revision C.02 edn. Gaussian Inc., Wallingford CT
48. Becke AD (1993) Density-functional thermochemistry. III. The role of exact exchange. J Chem Phys 98:5648–5652
49. Lee C, Yang W, Parr RG (1988) Development of the Colle–Salvetti correlation-energy formula into a functional of the electron density. Phys Rev B 37:785–789
50. Chaloner PA, Gunatunga SR, Hitchcock PB (1994) Redetermination of 2,2′-bithiophene. Acta Crystallogr Sect C: Cryst Struct Commun 50:1941–1942
51. Curtis MD, Cao J, Kampf JW (2004) Solid-state packing of conjugated oligomers: from π-stacks to the herringbone structure. J Am Chem Soc 126:4318–4328
52. Reimers JR (2001) A practical method for the use of curvilinear coordinates in calculations of normal-mode-projected displacements and Duschinsky rotation matrices for large molecules. J Chem Phys 115:9103–9109
53. Lin SH, Bersohn R (1968) Effect of partial deuteration and temperature on triplet-state lifetimes. J Chem Phys 48:2732–2736